Lower-Hybrid Drift Instability in Modified Harris Current Sheet*

HU Youjun (胡友俊), YANG Weihong (杨维纮), CHEN Yinhua (陈银华),
HUANG Feng (黄凤), WANG Feihu (王飞虎), ZHANG Yu (张羽),
WANG Dong (王栋)

CAS Key Laboratory of Basic Plasma Physics, Department of Modern Physics,
University of Science and Technology of China, Hefei 230026, China

Abstract Lower-hybrid drift instability (LHDI) in a Harris current sheet including a uniform background distribution is investigated in linear local kinetic theory. It is found that the introduction of a uniform background distribution reduces the growth rate and real frequency of LHDI at all wavelengths. Some physical explanations about the effects of the background distribution are provided.

Keywords: lower-hybrid drift instability, current sheet, kinetic theory

PACS: *52.35.Hr, 52.35 Qz, 94.30.-d, 94.30.Gm*

1 Introduction

Lower-hybrid drift instability (LHDI) is a high frequency instability ($\Omega_{\rm i} \ll \omega \ll |\Omega_{\rm e}|$, here $\Omega_{\rm i}$ and $\Omega_{\rm e}$ are the ion and electron gyrofrequencies, respectively) driven by the cross-field current in the presence of inhomogeneities in density $n_0(x)$ and magnetic field $B_0(x)\mathbf{e}_z$. It has a maximum growth rate when $k_z = 0$ and $k_y\rho_{\rm e} \sim 1$. Here k_z and k_y are wave vectors parallel to and perpendicular to magnetic field, respectively. $\rho_{\rm e} = v_{\rm te}/|\Omega_{\rm e}|$ is the electron thermal cyclotron radius. The interest in LHDI is motivated by its role in anomalous resistivity and transport. Early theories on LHDI were developed for applications to laboratory devices and collisionless shocks [1~3]. It was also suggested that LHDI might be the source of anomalous resistivity in the magnetotail [4]. Many of the works on LHDI in the magnetotail were based on the Harris current sheet [5] which is the simplest one-dimension equilibrium with an antiparallel magnetic field on the two sides and a maximum density and current at the center. Harris current sheet has a zero asymptotic density at large distance from the center. Both the ions and electrons in Harris current sheet have a uniform drift velocity across the current sheet. On the other hand, there has been some observational evidences which indicates that a static and uniform background population may exist in a real current sheet [6,7]. So a Harris current sheet with a background population may provide a better representation of the magnetotail. DAUGHTON [8] noticed that a uniform background population often exists in the kinetic simulation of Harris current sheet which may play important roles in the dynamics of the current sheet. He analysed the effects of this background population in linear nonlocal kinetic theory and found that the background population can excite the so-called Ion-Ion kink instability. Later, a longer wavelength LHDI instability with $k\sqrt{\rho_{\rm e}\rho_{\rm i}} \sim 1$ in a Harris current sheet with a uniform background population was analyzed [9]. The results show that the growth rates for both the odd- and even-parity modes of this long wavelength LHDI are rapidly suppressed by the uniform background population. Although it was also suggested that the uniform background population may suppress the traditional short wavelength LHDI [9], the conclusion was based on an approximate formula with the conditions of $T_{\rm e} \sim 0$, $T_{\rm e} \ll T_{\rm i}$, $U_{\rm i} < v_{\rm ti}$ (where $U_{\rm i}$ is the ion diamagnetic drift velocity). These conditions are usually not appropriate for those observed in the magnetotail. In this paper, based on the linearized Maxwell-Vlasov system and in the framework of local theory, we derive a dispersion relation for the traditional short wavelength LHDI by taking into account the effect of the background population. The equilibrium configuration adopted in the present study is a Harris current sheet with a uniform background population which we call modified Harris current sheet. The results of our analysis indicate that this uniform background population has a stabilizing effect on LHDI at all wavelengths.

This paper is organized as follows. In section 2 the equilibrium model used in this study is discussed. The local dispersion relation for LHDI is derived in section 3. Then, in section 4 detailed numerical solutions to the dispersion relation are presented. Conclusions are given in section 5.

2 Harris current sheet equilibrium

The near-Earth current sheet can be described by a variety of possible equilibria. Among the various one-dimensional equilibria, the Harris equilibrium [5] is the

*supported by National Natural Science Foundation of China (Nos. 10775134, 40336052)

simplest one. Our analysis is restricted to this classic equilibrium, but with a slight alteration introduced later. The magnetic field is along z-direction,

$$\mathbf{B}_0(x) = B_{\rm z}(x)\mathbf{e}_z = b_0 {\rm tanh}(\frac{x}{L})\mathbf{e}_z, \tag{1}$$

and a cross-field current in the y-direction,

$$J_y = \frac{cb_0}{4\pi L}{\rm sech}^2(\frac{x}{L}), \tag{2}$$

where c is the speed of light in vacuum. The constants of motion for a charged particle moving in the specified magnetic field are $v_\perp^2 = v_x^2 + v_y^2$, v_z and $p_y = v_y + qA_y/m_{\rm s}c$ (where $A_y = \int B_z(x){\rm d}x$). The equilibrium distribution function built up from these constants of motion may be expressed as,

$$f_{0\alpha} = \frac{n_0(x)}{\pi^{3/2}v_{{\rm t}\alpha}^3}\exp\Big[-\frac{v_x^2+(v_y-U_\alpha)^2+v_z^2}{v_{{\rm t}\alpha}^2}\Big], \tag{3}$$

where U_α is the drift velocity, $v_{{\rm t}\alpha} = (2T_\alpha/m_\alpha)^{1/2}$ is the thermal velocity, $\alpha = {\rm i}$, e for ions and electrons respectively, and the density profile is given by

$$n_0(x) = N_0{\rm sech}^2(\frac{x}{L}), \tag{4}$$

with N_0 and b_0 being related by the relation, $N_0(T_{\rm i}+T_{\rm e}) = b_0^2/8\pi$. To enforce charge neutrality, one must require $U_{\rm i}/T_{\rm i} = -U_{\rm e}/T_{\rm e}$ and U_α is related to L by

$$U_\alpha = -\frac{2cT_\alpha}{Lb_0q_\alpha}. \tag{5}$$

Note that although the density decreases exponentially in space, the drift velocities are independent of the spatial location. It is a uniform constant across the sheet.

The Harris current sheet equilibrium, which is an exact solution to Vlasov-Maxwell equations, is a equilibrium model frequently used in stability analysis [10,11]. In the present paper, following DAUGHTON [8,9], we modify the standard Harris current sheet by including a uniform background population for electrons and ions of the form

$$f_{{\rm b}\alpha} = \frac{n_{\rm b}}{\pi^{3/2}v_{{\rm t}\alpha}^3}\exp\Big(-\frac{v_x^2+v_y^2+v_z^2}{v_{{\rm t}\alpha}^2}\Big), \tag{6}$$

so that the standard Harris current sheet distribution function is modified to $f_{0\alpha}+f_{{\rm b}\alpha}$, which is also an exact solution to the Vlasov equation. This uniform background population does not contribute to the plasma current and it also ensures charge neutrality, so that it does not destroy the equilibrium discussed above. With this modification the density of the combined distributions goes to a nonzero constant in the farther region (not as standard Harris equilibrium to zero in the farther region). We think that this is a better representation of magnetotail which is essentially a transition layer between two uniform regions.

3 Stability analysis

The stability of the standard Harris equilibrium described in section 2 is analysed using the linearized Vlasov equation,

$$\frac{\partial f_{1\alpha}}{\partial t} + \mathbf{v}\cdot\nabla f_{1\alpha} + \frac{\mathbf{v}\times\mathbf{B}_0}{c}\cdot\nabla_{\rm v} f_{1\alpha} = -\frac{q_\alpha}{m_\alpha}\Big(\mathbf{E}_1 + \frac{\mathbf{v}\times\mathbf{B}_1}{c}\Big)\cdot\nabla_{\rm v} f_{0\alpha}, \tag{7}$$

where $\mathbf{B}_0$ is given by Eq. (1) and $f_{0\alpha}$ is given by Eq. (3). The perturbed electromagnetic fields are described by the scalar potential ϕ and vector potential $\mathbf{A}$,

$$\mathbf{E}_1 = -\nabla\phi - \frac{1}{c}\frac{\partial\mathbf{A}}{\partial t},$$
$$\mathbf{B}_1 = \nabla\times\mathbf{A}, \tag{8}$$

where

$$\phi = \hat{\phi}(x)\exp\Big[i(k_y y + k_z z - \omega t)\Big],$$
$$\mathbf{A} = \hat{\mathbf{A}}(x)\exp\Big[i(k_y y + k_z z - \omega t)\Big]. \tag{9}$$

Integrating the Vlasov equation along the unperturbed particle orbits, we can obtain the perturbed distribution function $f_{1\alpha}$,

$$\begin{aligned} &f_{1\alpha}(x, v_x, v_y, v_z) \\ &= -\frac{q_\alpha f_{0\alpha}}{T_\alpha}\Bigg\{\hat{\phi}(x) - \frac{U_\alpha}{c}\hat{A}_{\rm y}(x) + i(\omega - k_y U_\alpha) \\ &\quad\times\int_{-\infty}^{0}\Big[\hat{\phi}(x') - \frac{\mathbf{v}'\cdot\hat{\mathbf{A}}(x')}{c}\Big]\exp\Big[ik_y(y'-y) \\ &\quad + ik_z(z'-z) - i\omega\tau\Big]{\rm d}\tau\Bigg\}, \end{aligned} \tag{10}$$

where $\tau = t' - t$, $x'(t')$, $y'(t')$, $z'(t')$, $v_x'(t')$, $v_y'(t')$, $v_z'(t')$ are along the unperturbed orbits and must be given as functions of t' or τ. The boundary conditions at $t' = t$ or $\tau = 0$ are $x' = x$, $y' = y$, $z' = z$, $v_x' = v_x$, $v_y' = v_y$ and $v_z' = v_z$.

In the local approximation, it is assumed that $\hat{\rm A}(x')$ and $\hat{\phi}(x')$ can be taken out of the orbit integral, so that

$$\begin{aligned} &f_{1\alpha}(x, v_x, v_y, v_z) \\ &= -\frac{q_\alpha f_{0\alpha}}{T_\alpha}\Bigg\{\hat{\phi}(x) - \frac{U_\alpha}{c}\hat{A}_{\rm y}(x) + i(\omega - k_{\rm y}U_\alpha)\hat{\phi}(x) \\ &\quad\times\int_{-\infty}^{0}\exp\Big[ik_{\rm y}(y'-y) + ik_{\rm z}(z'-z) - i\omega\tau\Big]{\rm d}\tau \\ &\quad -\frac{1}{c}i(\omega - k_y U_\alpha)\hat{\mathbf{A}}(x)\cdot\int_{-\infty}^{0}\mathbf{v}'\exp\Big[ik_{\rm y}(y'-y) \\ &\quad + ik_{\rm z}(z'-z) - i\omega\tau\Big]{\rm d}\tau\Bigg\}. \end{aligned} \tag{11}$$

3.1 Perturbed density and current of current-carrying electrons

Unperturbed orbits of electrons are approximately given by a cyclotron motion with a ∇B drift. Using these orbits and the low frequency approximation ($|\omega| \ll |\Omega_{\rm e}|$), the perturbed electron density can be obtained as

$$\begin{aligned} n_{1\rm e}(x) &= \int f_{1\rm e}(x,v_x,v_y,v_z){\rm d}\mathbf{v} \\ &= \frac{en_0(x)}{T_{\rm e}}\Bigg\{\hat{\phi}(x)+\frac{k_zU_{\rm e}}{k_yc}\hat{A}_{\rm z}(x)+i(\omega-k_yU_{\rm e}) \\ &\times\frac{2}{k_zv_{\rm te}^3}\Bigg[\hat{\phi}(x)\int_0^\infty -iv_\perp e^{-v_\perp^2/v_{\rm te}^2}J_0^2Z(\xi_{\rm e}){\rm d}v_\perp \\ &+\hat{A}_x(x)\int_0^\infty -\frac{v_\perp^2}{c}e^{-v_\perp^2/v_{\rm te}^2}J_0J_1Z(\xi_{\rm e}){\rm d}v_\perp \\ &+\hat{A}_z(x)\int_0^\infty iv_\perp e^{-v_\perp^2/v_{\rm te}^2}J_0^2\Big(-\frac{v_{\rm te}}{c}\frac{Z'(\xi_{\rm e})}{2} \\ &-\frac{k_z}{k_y}\frac{v_{\nabla B}}{c}Z(\xi_{\rm e})\Big){\rm d}v_\perp\Bigg]\Bigg\}, \end{aligned} \tag{12}$$

where J_0, J_1 are the Bessel functions of the first kind with argument $k_yv_\perp/\Omega_{\rm e}$. $Z(\xi_{\rm e})$ is the plasma dispersion function [12,13] and $Z'(\xi_{\rm e}) = -2\Big[1+\xi_{\rm e}Z(\xi_{\rm e})\Big]$, $\xi_{\rm e} = (\omega-k_yv_{\nabla B})/(k_zv_{\rm te})$, $\Omega_{\rm e} = -B_0(x)e/(m_{\rm e}c)$, $v_{\nabla B} = \varepsilon_{\rm B}v_\perp^2/(2\Omega_{\rm e})$, $\varepsilon_{\rm B} = B_0'(x)/B_0(x)$.

In obtaining Eq. (12) we expand Eq. (3) in velocity space as,

$$f_{0\alpha} = \frac{n_0(x)}{\pi^{3/2}v_{\rm te}^3}(1+\frac{2U_{\rm e}v_y}{v_{\rm te}^2})\exp\Big(-\frac{v_x^2+v_y^2+v_z^2}{v_{\rm te}^2}\Big).$$

This expansion is valid when $|U_{\rm e}| \ll v_{\rm te}$ which is usually satisfied by electrons but not by ions. In addition, we used the Coulomb gauge $\nabla\cdot\mathbf{A}=0$ to replace $\hat{A}_y$ with $k_z\hat{A}_z/k_y$ and neglected the term $\partial A/\partial x$.

Similarly we can derive the expressions for the perturbed electron current density,

$$\begin{aligned} J_{ex}(x) &= -e\int v_xf_{1\rm e}{\rm d}\mathbf{v} \\ &= -\frac{e^2n_0(x)}{T_{\rm e}}i(\omega-k_yU_{\rm e})\frac{2}{k_zv_{\rm te}^3}\int_0^\infty e^{-v_\perp^2/v_{\rm te}^2}v_\perp^2{\rm d}v_\perp \\ &\times\Big\{-J_0J_1Z(\xi_{\rm e})\hat{\phi}+iJ_1^2\frac{v_\perp}{c}Z(\xi_{\rm e})\hat{A}_x+J_0J_1 \\ &\times\Big[-\frac{k_z}{k_y}\frac{v_{\nabla B}}{c}Z(\xi_{\rm e})-\frac{v_{\rm te}}{c}\frac{Z'(\xi_{\rm e})}{2}\Big]\hat{A}_z\Big\}, \end{aligned} \tag{13}$$

$$\begin{aligned} J_{ez}(x) &= -e\int v_zf_{1\rm e}{\rm d}\mathbf{v} \\ &= -\frac{e^2n_0(x)}{T_{\rm e}}i(\omega-k_yU_{\rm e})\frac{2}{k_zv_{\rm te}^2}\int_0^\infty e^{-v_\perp^2/v_{\rm te}^2}v_\perp{\rm d}v_\perp \\ &\times\Big\{iJ_0^2\frac{Z'(\xi_{\rm e})}{2}\hat{\phi}+J_0J_1\frac{v_\perp}{c}\frac{Z'(\xi_{\rm e})}{2}\hat{A}_x \\ &+iJ_0^2\Big[\frac{k_z}{k_y}\frac{v_{\nabla B}}{c}\frac{Z'(\xi_{\rm e})}{2}-\frac{v_{\rm te}}{c}\xi_{\rm e}\frac{Z'(\xi_{\rm e})}{2}\Big]\hat{A}_z\Big\}. \end{aligned} \tag{14}$$

3.2 Perturbed density of current-carrying ions

The frequency $|\omega|$ of LHDI is much larger than the ion cyclotron frequency $\Omega_{\rm i}$. In one wave period, the unperturbed ion orbits are well approximated by a straight line. Thus we can treat ions as unmagnetized. In addition, for LHDI, it is adequate to consider ion's response to the scalar potential only, and neglect its response to the vector potential [14]. From Eq. (11), we get,

$$f_{1\rm i} = -\frac{ef_{0\rm i}}{T_{\rm i}}\hat{\phi}\Big(1+\frac{\omega-k_yU_{\rm i}}{k_yv_y+k_zv_{\rm z}-\omega}\Big). \tag{15}$$

Integrating $f_{1\rm i}$ in velocity space, we get the perturbed ion density,

$$\begin{aligned} n_{1\rm i}(x) &= \int f_{1\rm i}{\rm d}\mathbf{v} = -\frac{en_0(x)}{T_{\rm i}}\hat{\phi} \\ &\times\Big[1+\frac{\omega-k_yU_{\rm i}}{k_yv_{\rm ti}^2}\frac{1}{\sqrt{\pi}}\int_{-\infty}^{+\infty}e^{-v_z^2/v_{\rm ti}^2}Z(\xi_{\rm i}){\rm d}v_z\Big] \end{aligned} \tag{16}$$

with $\xi_{\rm i} = (\omega-k_yU_{\rm i}-k_zv_z)/(k_yv_{\rm ti})$.

The ion's contribution to the perturbed current is neglected due to its smallness compared with the electron's .

3.3 Perturbed density of background electrons and ions

So far we have not included a background population yet. When a uniform background population is introduced, we must take into account its contribution to perturbed density and current. By setting $U_\alpha = 0$ and replacing $n_0(x)$ with $n_{\rm b}$ in Eqs. (12)$\sim$(14) and (16), we can obtain the contribution of the background distribution. For example, the perturbed electron density of background distribution is given by,

$$\begin{aligned} &n_{\rm b1e}(x) \\ &= \frac{en_{\rm b}}{T_{\rm e}}\hat{\phi}+\frac{en_{\rm b}}{T_{\rm e}}\frac{2i\omega}{k_zv_{\rm te}^3}\Bigg\{\hat{\phi}\int_0^\infty -iv_\perp e^{-v_\perp^2/v_{\rm te}^2}J_0^2Z(\xi_{\rm e}){\rm d}v_\perp \\ &+\hat{A}_x\int_0^\infty -\frac{v_\perp^2}{c}e^{-v_\perp^2/v_{\rm te}^2}J_0J_1Z(\xi_{\rm e}){\rm d}v_\perp \\ &+\hat{A}_z\int_0^\infty iv_\perp e^{-v_\perp^2/v_{\rm te}^2}J_0^2\Bigg[-\frac{v_{\rm te}}{c}\frac{Z'(\xi_{\rm e})}{2} \\ &-\frac{k_z}{k_y}\frac{v_{\nabla B}}{c}Z(\xi_{\rm e}){\rm d}v_\perp\Bigg]\Bigg\}, \end{aligned} \tag{17}$$

while the perturbed ion density of background distribution is given by,

$$n_{\rm b1i} = -\frac{en_{\rm b}}{T_{\rm i}}\hat{\phi}\Big[1+\frac{\omega}{k_yv_{\rm ti}^2}\frac{1}{\sqrt{\pi}}\int_{-\infty}^{+\infty}e^{-v_z^2/v_{\rm ti}^2}Z(\xi_{\rm bi}){\rm d}v_z\Big], \tag{18}$$

with $\xi_{\rm bi} = (\omega-k_zv_z)/(k_yv_{\rm ti})$.

3.4 Dispersion relation

Using the Coulomb gauge $\nabla \cdot \mathbf{A} = 0$ and neglecting the displacement current ($\omega \ll kc$), Maxwell's equations then take the form,

$$\nabla^2 \phi = -4\pi\rho, \tag{19}$$

$$\nabla^2 \mathbf{A} = -\frac{4\pi}{c}\mathbf{J}. \tag{20}$$

From Eq. (19) and the x, z components of Eq. (20), we get,

$$\begin{aligned} k^2\hat{\phi} &= 4\pi e(n_{1\mathrm{i}} - n_{1\mathrm{e}}), \\ k^2\hat{A}_x &= \frac{4\pi}{c}J_{\mathrm{e}x}, \\ k^2\hat{A}_z &= \frac{4\pi}{c}J_{\mathrm{e}x}, \end{aligned} \tag{21}$$

where $k = \sqrt{k_y^2 + k_z^2}$.

For later use, we write $n_{1\mathrm{i}}$, $n_{1\mathrm{e}}$, $J_{\mathrm{e}x}$, $J_{\mathrm{e}z}$ as,

$$\begin{aligned} n_{1\mathrm{i}}(x) &= \chi_\phi^{\mathrm{i}}\hat{\phi}, \\ n_{1\mathrm{e}}(x) &= \chi_\phi^{\mathrm{e}}\hat{\phi} + \chi_x^{\mathrm{e}}\hat{A}_x + \chi_z^{\mathrm{e}}\hat{A}_z, \\ J_{\mathrm{e}x}(x) &= \sigma_\phi^x\hat{\phi} + \sigma_x^x\hat{A}_x + \sigma_z^x\hat{A}_z, \\ J_{\mathrm{e}z}(x) &= \sigma_\phi^z\hat{\phi} + \sigma_x^z\hat{A}_x + \sigma_z^z\hat{A}_z. \end{aligned} \tag{22}$$

Comparing Eq. (22) with the expressions of perturbed density and current, we can write down the expressions of χ_ϕ^{i}, χ_ϕ^{e}, χ_x^{e}, χ_z^{e}, σ_ϕ^x, σ_x^x, σ_z^x, σ_ϕ^y, σ_x^y, σ_z^y, σ_ϕ^z, σ_x^z, σ_z^z. For example, χ_ϕ^{i} takes the form,

$$\chi_\phi^{\mathrm{i}} = -\frac{en_0(x)}{T_{\mathrm{i}}}\Big[1+\frac{\omega - k_y U_{\mathrm{i}}}{k_y v_{\mathrm{ti}}^2}\frac{1}{\sqrt{\pi}}\int_{-\infty}^{+\infty} e^{-v_\perp^2/v_{\mathrm{ti}}^2} Z(\xi_{\mathrm{i}})\mathrm{d}v_z\Big]$$

$$-\frac{en_{\mathrm{b}}}{T_{\mathrm{i}}}\Big[1 + \frac{\omega}{k_y v_{\mathrm{ti}}^2}\frac{1}{\sqrt{\pi}}\int_{-\infty}^{+\infty} e^{-v_\perp^2/v_{\mathrm{ti}}^2} Z(\xi_{\mathrm{bi}})\mathrm{d}v_z\Big]. \tag{23}$$

In the local theory, we must first set the location of x to evaluate χ_ϕ^{i}, χ_ϕ^{e}, χ_x^{e}, χ_z^{e}, σ_ϕ^x, σ_x^x, σ_z^x, σ_ϕ^y, σ_x^y, σ_z^y, σ_ϕ^z, σ_x^z, σ_z^z. Then, from Eq. (21), we get the dispersion relation,

$$\begin{vmatrix} D_{11} & D_{12} & D_{13} \\ D_{21} & D_{22} & D_{23} \\ D_{31} & D_{32} & D_{33} \end{vmatrix} = 0, \tag{24}$$

with D_{ij} given by

$$\begin{aligned} &D_{11} = \frac{4\pi e}{k^2}(\chi_\phi^{\mathrm{e}} - \chi_\phi^{\mathrm{i}}) + 1,\ D_{12} = \frac{4\pi e}{k^2}\chi_x^{\mathrm{e}},\ D_{13} = \frac{4\pi e}{k^2}\chi_z^{\mathrm{e}}, \\ &D_{21} = \frac{4\pi}{ck^2}\sigma_\phi^x, \quad D_{22} = \frac{4\pi}{ck^2}\sigma_x^x - 1, \quad D_{23} = \frac{4\pi}{ck^2}\sigma_z^x, \\ &D_{31} = \frac{4\pi}{ck^2}\sigma_\phi^z,\ D_{32} = \frac{4\pi}{ck^2}\sigma_x^z,\ D_{33} = \frac{4\pi}{ck^2}\sigma_z^z - 1. \end{aligned} \tag{25}$$

4 Numerical results

In this section, the LHDI dispersion relation in Eq. (24) is solved numerically and the effects of the background population are investigated.

The modified current sheet considered in the present study is completely characterized by the following four dimensionless parameters,

$$\frac{n_{\mathrm{b}}}{N_0},\ \frac{U_{\mathrm{i}}}{v_{\mathrm{ti}}},\ \frac{T_{\mathrm{i}}}{T_{\mathrm{e}}},\ \frac{\omega_{\mathrm{pe}}^2(0)}{\Omega_{\mathrm{e}}^2(\infty)},$$

where $\omega_{\mathrm{pe}}(0) = \sqrt{4\pi e^2 N_0/m_{\mathrm{e}}}$ is the electron plasma frequency calculated from the peak density N_0; $\Omega_{\mathrm{e}}(\infty) = b_0 e/m_{\mathrm{e}}c$ is the electron gyrofrequency calculated from the asymptotic magnetic field b_0. In the following, unless explicitly specified, we fix the parameters as

$$\frac{U_{\mathrm{i}}}{v_{\mathrm{ti}}} = -1,\ \frac{T_{\mathrm{i}}}{T_{\mathrm{e}}} = 5,\ \frac{\omega_{\mathrm{pe}}^2(0)}{\Omega_{\mathrm{e}}^2(\infty)} = 16. \tag{26}$$

These equilibrium parameters are roughly appropriate for conditions observed in the magnetotail [15,16]. In order to investigate the effects of the background population, we choose different values of n_{b}/N_0 to evaluate the growth rate at a spatial location within the current sheet.

In this paper the complex wave frequency ω is normalized by the local ion cyclotron frequency Ω_{i}, and wave vectors k_y, k_z by local electron gyro-radius $\rho_{\mathrm{e}} = v_{\mathrm{te}}/|\Omega_{\mathrm{e}}|$.

First a comparison of our numerical solution with the previous results is presented. In Fig. 1 we plot the growth rate and corresponding real frequency as a function of $k_y\rho_{\mathrm{e}}$, with parameters of $x = 0.88$ L, $k_z\rho_{\mathrm{e}} = 0.002$, $n_{\mathrm{b}}/N_0 = 0$, $T_{\mathrm{i}}/T_{\mathrm{e}} = 1$, $U_{\mathrm{i}}/v_{\mathrm{ti}} = -1$ and $\omega_{\mathrm{pe}}^2(0)/\Omega_{\mathrm{e}}^2(\infty) = 125$. In Fig. 2 we compare our results with those in Ref. [2]. The parameters are set by closely following the conditions of Fig. 3 in Ref. [2]. However, there is something that needs to be clarified. First, although the work of Ref. [2] is not based on the

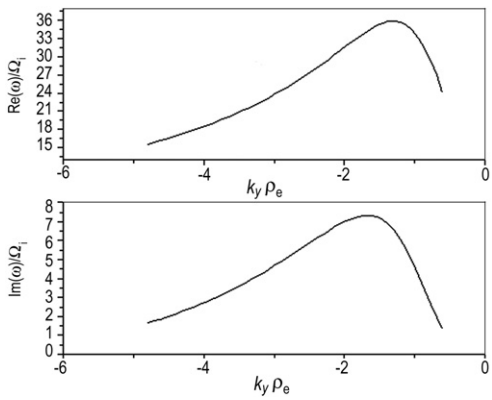

Fig.1 Plots of $\mathrm{Re}(\omega)/\Omega_{\mathrm{i}}$ and $\mathrm{Im}(\omega)/\Omega_{\mathrm{i}}$ versus $k_y\rho_{\mathrm{e}}$ with parameters of $x = 0.88$ L, $k_z\rho_{\mathrm{e}} = 0.002$, $n_{\mathrm{b}}/N_0 = 0$, $T_{\mathrm{i}}/T_{\mathrm{e}} = 1$, $U_{\mathrm{i}}/v_{\mathrm{ti}} = -1$ and $\omega_{\mathrm{pe}}^2(0)/\Omega_{\mathrm{e}}^2(\infty) = 125$

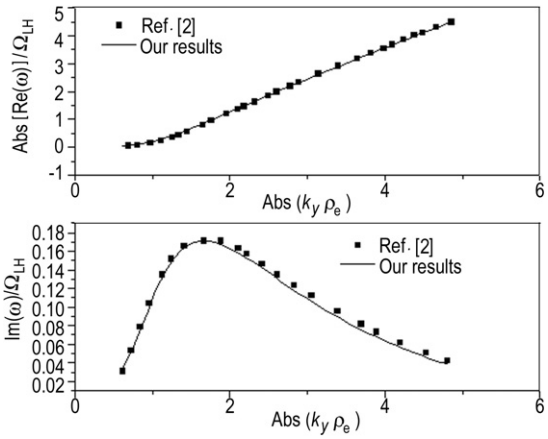

Fig.2 Plots of $\mathrm{Im}(\omega)/\Omega_{\mathrm{LH}}$ and $|\mathrm{Re}(\omega)|/\Omega_{\mathrm{LH}}$ versus $|k_y|\rho_{\mathrm{e}}$ with the same parameters as in Fig. 1. Note that the Doppler frequency shift $-k_yU_{\mathrm{i}}$ has been added to the real frequency. The local parameters at this spatial location are $\beta_{\mathrm{i}} = 0.5$, $\omega_{\mathrm{pe}}^2/\Omega_{\mathrm{ce}}^2 = 125$, where $\beta_{\mathrm{i}} = 8\pi n_0(x)T_{\mathrm{i}}/B_0^2(x)$, These are exactly the same parameters of Fig. 3 in Ref. [2]

Harris current sheet equilibrium, from the given local parameters in Ref. [2], we can infer that this case actually corresponds to a Harris current sheet with the following global parameters:

$$\frac{n_{\mathrm{b}}}{N_0} = 0,\ \frac{U_{\mathrm{i}}}{v_{\mathrm{ti}}} = -1,\ \frac{T_{\mathrm{i}}}{T_{\mathrm{e}}} = 1,\ \frac{\omega_{\mathrm{pe}}^2(0)}{\Omega_{\mathrm{e}}^2(\infty)} = 125, \qquad (27)$$

and the spatial location at which the dispersion relation is evaluated is $x = 0.88\ L$. Second, the normalization in Ref. [2] is a little different from the method adopted in the present paper. The complex frequency is normalized by lower-hybrid frequency $\Omega_{\mathrm{LH}} \approx \sqrt{\Omega_{\mathrm{i}}|\Omega_{\mathrm{e}}|}$. Third, in Fig. 3 of Ref. [2], the coordinate is set in the ion reference frame, so that the ions have a zero drift velocity in this reference frame. In the present paper, our equilibrium configuration determines that we are in a reference frame in which both ions and electrons have drifts. Therefore, we must add a Doppler frequency shift $-k_yU_{\mathrm{i}}$ to the real frequency to compare our results with Ref. [2]. The comparison in Fig. 2 shows that our results are in excellent agreement with the results of Ref. [2] after being transformed to the ion reference frame.

In Figs. 3∼5, the growth rate of LHDI and the corresponding real frequency are plotted as a function of k_y for different values of $\Delta \equiv n_{\mathrm{b}}/N_0$ and spatial locations.

From Figs. 3∼5, some basic properties of LHDI can be deduced. For example, the real frequency is approximately in the range $\mathrm{Re}(\omega) \sim 40\Omega_{\mathrm{i}} \sim \sqrt{\Omega_{\mathrm{e}}\Omega_{\mathrm{i}}}$ ($\omega_{\mathrm{LH}} \approx \sqrt{\Omega_{\mathrm{i}}\Omega_{\mathrm{e}}}$ is the lower-hybrid frequency). Another basic property of the traditional LHDI is that it is a short wavelength instability, with the typical wavelength on the electron gyroscale $k_y\rho_{\mathrm{e}} \sim 1$. From Fig. 3 we can see that the growth rate curve peaks around $|k_y|\rho_{\mathrm{e}} \sim 1$. (Note that in Figs. 3∼5, k_y is negative because we set the wave vector component k_y along the ion drift velocity which is in the negative y direction). In addition, LHDI is a flute instability which has the maximum growth rate when $k_{\mathrm{z}}/k_{\mathrm{y}} \to 0$, i.e., when the

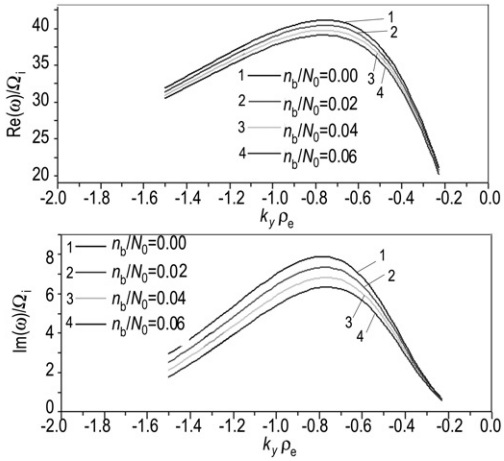

Fig.3 Growth rate $\mathrm{Im}(\omega)/\Omega_{\mathrm{i}}$ (lower) and the corresponding real frequency $\mathrm{Re}(\omega)/\Omega_{\mathrm{i}}$ (upper) as a function of $k_y\rho_{\mathrm{e}}$ with $\Delta = n_{\mathrm{b}}/N_0 = 0.00,\ 0.02,\ 0.04,\ 0.06$ as a parameter. The other parameters are $x = 0.8\ L$, $k_z\rho_{\mathrm{e}} = 0.003$, $T_{\mathrm{i}}/T_{\mathrm{e}} = 5$, $U_{\mathrm{i}}/v_{\mathrm{ti}} = -1$, $\omega_{\mathrm{pe}}^2(0)/\Omega_{\mathrm{e}(\infty)}^2 = 16$

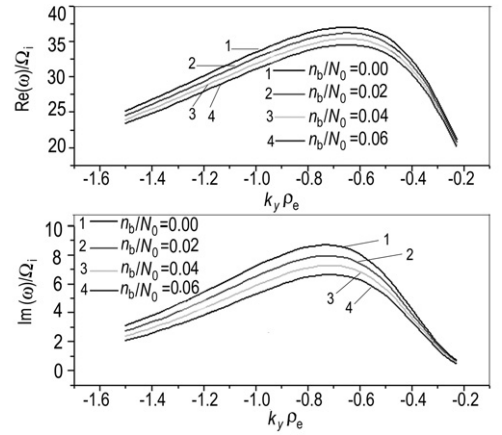

Fig.4 Growth rate $\mathrm{Im}(\omega)/\Omega_{\mathrm{i}}$ (lower) and the corresponding real frequency $\mathrm{Re}(\omega)/\Omega_{\mathrm{i}}$ (upper) as a function of $k_{\mathrm{y}}\rho_{\mathrm{e}}$ with $\Delta = n_{\mathrm{b}}/N_0 = 0.00,\ 0.02,\ 0.04,\ 0.06$ as a parameter. The other parameters are $x = 1.0\ L$, $k_z\rho_{\mathrm{e}} = 0.003$, $T_{\mathrm{i}}/T_{\mathrm{e}} = 5$, $U_{\mathrm{i}}/v_{\mathrm{ti}} = -1$, $\omega_{\mathrm{pe}}^2(0)/\Omega_{\mathrm{e}(\infty)}^2 = 16$

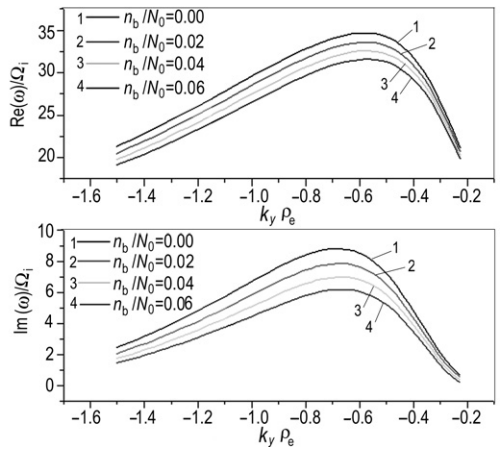

Fig.5 Growth rate $\mathrm{Im}(\omega)/\Omega_{\mathrm{i}}$ (lower) and the corresponding real frequency $\mathrm{Re}(\omega)/\Omega_{\mathrm{i}}$ (upper) as a function of $k_y\rho_{\mathrm{e}}$ with $\Delta = n_{\mathrm{b}}/N_0 = 0.00,\ 0.02,\ 0.04,\ 0.06$ as a parameter. The other parameters are $x = 1.2\ L$, $k_z\rho_{\mathrm{e}} = 0.003$, $T_{\mathrm{i}}/T_{\mathrm{e}} = 5$, $U_{\mathrm{i}}/v_{\mathrm{ti}} = -1$, $\omega_{\mathrm{pe}}^2(0)/\Omega_{\mathrm{e}(\infty)}^2 = 16$

wave vector is perpendicular to $\mathbf{B}_0$. So in the above we have chosen $k_z\rho_e = 0.003$, and in the whole range of k_y, the ratio $k_z/|k_y|$ is a small quantity (in Figs. 3∼5 the minimum value of $|k_y|\rho_e$ is 0.2).

We now investigate how the properties of LHDI are influenced by the background population. As shown in Figs. 3∼5, the growth rate and real frequency are reduced at all wavelengths by the introduction of the background population (where, the case of $\Delta = n_b/N_0 = 0.0$ corresponding with no background population). With Δ increasing, the growth rate and real frequency are both reduced.

The result is not unexpected. It agrees with the physical intuition that the relative drift between ions and electrons are the driving source of LHDI. The static background population reduces the average drift velocity of electrons and ions, and therefore reduces the relative drift between electrons and ions. Consequently, the energy source of LHDI is reduced which results in the reduction in the growth rate. In Fig. 3 we evaluated the dispersion relation at the spatial location $x = 0.8\ L$. When $n_b/N_0 = 0.0$ (i.e. the background population is not included), the relative drift between ions and electrons at this spatial point is $(U_e - U_i)/v_{ti} = 1.20$. When $n_b/N_0 = 0.06$ the relative drift at this spatial point drops to $(U_e - U_i)/\left\{v_{ti}\left[1 + n_b/n_0(x)\right]\right\} = 1.08$. In Fig. 4 we evaluated the dispersion relation at the spatial location $x = 1.0\ L$. When $n_b/N_0 = 0.0$, the relative drift between ions and electrons at this spatial location is $(U_e - U_i)/v_{ti} = 1.20$. When $n_b/N_0 = 0.06$ the relative drift at this spatial location drops to $(U_e - U_i)/\left\{v_{ti}\left[1 + n_b/n_0(x)\right]\right\} = 1.04$.

The conclusion also agrees with the results in the previous literature that β has a stabilizing effect on LHDI [2] (where $\beta = 8\pi n_0(T_i + T_e)/B_0^2$, is the ratio of thermal pressure to magnetic pressure). The background population leads to an increase in local thermal pressure, but does not influence the local magnetic pressure, and therefore increases local β which is stabilizing for LHDI. In Fig. 5 we evaluated the dispersion relation at the spatial location $x = 1.2\ L$. When $n_b/N_0 = 0.0$ (i.e. the background population is not included), the local β for this spatial location is $1/\sin h^2(x) = 0.43$. When $n_b/N_0 = 0.06$, the β increases to $[1 + n_b/n_0(x)]/\sin h^2(x) = 0.52$.

5 Conclusion

In this paper, we investigated the properties of LHDI in the Harris current sheet with a uniform background population. The results show that the growth rate and real frequency of LHDI are reduced at all wavelengths due to the introduction of the background population. The uniform background population has a stabilizing effect on LHDI at all wavelengths.

These results can be attributed to two effects of the background population, i.e., the reduction in the average drift velocity between electrons and ions, and the increase in the local β.

Before we conclude this paper, we would like to make some remarks on the diamagnetic current. Although the average drift between ions and electrons is reduced due to the background population, the total diamagnetic current in the sheet remains unchanged. The total diamagnetic current is given by $J_{y0}(x) = en_0(x)(U_i - U_e)$, which is independent of the background population. The reduction in the average relative drift velocity between ions and electrons results in the reduction in the growth rate of LHDI. This indicates that the relative drift velocity between ions and electrons determines how fast the instability can grow. On the other hand, the total diamagnetic current is not directly related to the growth rate of LHDI. It determines the total energy source that can be given to LHDI in the process of nonlinear evolution of LHDI.

References

1 Krall N A, Liewer P C. 1971, Phys. Rev. A, 4: 2094
2 Davidson R C, Gladd N T, Wu C S, et al. 1977, Phys. Fluids, 20: 301
3 Hsia J B, Chiu S M, Hsia M F, et al. 1979, Phys. Fluids, 22: 1737
4 Huba J D, Gladd N T, Papadopoulos K. 1977, Geophys. Res. Lett., 4: 125
5 Harris E G. 1962, Nuovo Cimento, 23: 115
6 Karimabadi H, Daughton W, Pritchett P L, et al. 2003, J. Geophys. Res., 108(A11): 1400
7 Fuselier S A. 1995, Kinetic aspects of reconnection at the magnetopause, in Physics of the Magnetopause. Washington D. C.: American Geophysical Union. Geophys. Monogr. Ser., vol.90
8 Daughton W. 1999, Phys. Plasmas, 6: 1329
9 Daughton W. 2003, Phys. Plasmas, 10: 3103
10 Yoon P H, Lui A T Y. 2005, J. Geophys. Res., 110: A01202
11 Yoon P H, Lui A T Y. 2004, J. Geophys. Res., 109: A02210
12 Frid B D, Conte S D. 1961, The plasma dispersion function. New York: Academic Press
13 Stix T H. 1992, Waves in plasma. New York: American Institute of Physics
14 Farengo R, Guzdar P N, Lee Y C. 1989, Phys. Fluids B, 1: 1654
15 Sergeev V A, Mitchell D G, Russell C T, et al. 1993, J. Geophys. Res., 98: 17345
16 Daughton W, Giovanni L, Paolo R. 2004, Phys. Rev. Lett., 93: 105004

(Manuscript received 5 July 2007)
E-mail address of HU Youjun: yjunhu@mail.ustc.edu.cn